Journal of Solid State Chemistry 183 (2010) 2432–2437

Contents lists available at ScienceDirect

Journal of Solid State Chemistry

journal homepage: www.elsevier.com/locate/jssc

Eu doping effects on structural and magnetic properties of $(Sr_{2-x}Eu_x)FeMoO_6$ compounds

Q. Zhang [a], Y.G. Xiao [b], Z.F. Xu [a], G.Y. Liu [b], J.B. Li [b], G.H. Rao [b,*]

[a] Department of Mathematics and Physics, Shandong Jiaotong University, Jinan 250023, People's Republic of China
[b] Beijing National Laboratory for Condensed Matter Physics, Institute of Physics, Chinese Academy of Sciences, Beijing 100190, People's Republic of China

ARTICLE INFO

Article history:
Received 5 June 2010
Received in revised form
2 August 2010
Accepted 8 August 2010
Available online 13 August 2010

Keywords:
Double perovskite
Electron doping
Crystal structure
Magnetization
Metal–semiconductor transition

ABSTRACT

Double perovskite compounds $(Sr_{2-x}Eu_x)FeMoO_6$ ($0 \le x \le 0.3$) were prepared by solid-state reaction at high temperature. Crystal structure, magnetic and transport properties of the compounds were investigated. The crystal structure of the compounds changes from an $I4/m$ lattice to an $Fm\bar{3}m$ lattice around $x=0.1$. The unit-cell volume decreases with the doping level in both the $I4/m$ lattice and the $Fm\bar{3}m$ lattice. The resistivity of the compounds shows a metal–semiconductor transition, and the transition temperature T_{M-S} increases with the doping level. However, Curie temperature (T_C) of the compounds exhibits a weak dependence on the doping level. The saturation magnetization (M_S) at 100 K varies almost linearly with the anti-site defect concentration and agrees well with the simple FIM model. In contrast to the Ce-, Pr-, Nd- and Sm-doped Sr_2FeMoO_6, the difference of M_S of $(Sr_{2-x}Eu_x)FeMoO_6$ between 5 and 100 K indicates that the moment of Eu^{3+} is antiparellel to that of Fe^{3+} at low temperature.

1. Introduction

The interest in double perovskites of the type A_2FeMoO_6 has been renewed due to their half-metallic conduction and room-temperature magnetoresistance [1–4]. Intensive investigation has been focused on Sr_2FeMoO_6 (SFMO) owing to its exceptionally high ferromagnetic ordering temperature ($T_C \approx 420$ K) and appreciable room-temperature low-field magnetoresistance (LFMR) for potential applications in spintronics.

An ideal ordered SFMO consists of corner-shared FeO_6 and MoO_6 octahedra arranging alternately along all three directions with the voids among the octahedra being filled by larger Sr ions. Depending on the ionic radius of A cation, the structure has been described as cubic (A=Ba, space group $Fm\bar{3}m$), tetragonal (A=Sr, space group $I4/m$) or monoclinic lattice (A=Ca, space group $P2_1/n$) [5,6]. The magnetic structure of SFMO can be described by the simplest ferrimagnetic arrangement model (the FIM model) which assumes that the ordered array of parallel Fe^{3+} ($S=5/2$) spins couple antiferromagnetically with Mo^{5+} ($S=1/2$) spins [7]. Thus, a saturation magnetization (M_S) of 4 μ_B/f.u. is anticipated for an ideally ordered SFMO. However, the M_S of bulk materials reported so far is usually lower (3.1 μ_B/f.u. [1] 3.5 μ_B/f.u. [6]) than the FIM prediction mostly due to intrinsic anti-site defects (AS), i.e., small numbers of Fe and Mo atoms interchange sites.

Band-structure calculations have predicted that Sr_2FeMoO_6 is a half-metal [1,4], where the Mo t_{2g} spin-down sub-band (hybridized with the Fe t_{2g} spin-down sub-band) crosses the Fermi level, while the spin-up sub-band, essentially composed of Fe t_{2g} and Fe e_g states, is separated by an insulating gap. Therefore, electrons in the spin-down sub-band are itinerant, while electrons in the spin-up sub-band are localized. The itinerancy of the spin-down electrons results in the metallic conductivity and is responsible for the strong coupling between Fe spins and Mo spins via a double-exchange-like mechanism [2,8].

A high spin-polarization of conduction carriers is desired for the potential application of SFMO in magnetoresistive devices. As reported in Refs. [6,8], a relatively high spin-polarization of the conduction electrons can be achieved in the compounds with high T_C. Calculation by mean-field theory indicates that the strength of exchange interaction between Fe and Mo atoms is closely related to the electron density at Fermi level [9]. Thus, injection of electron into the conduction band by appropriate electron doping would be an effective way to increase T_C as well as spin-polarization of conduction carriers of SFMO. An electron doping can usually be attained by partially replacing Sr^{2+} with trivalent rare-earth ions [10–14]. In our previous studies on a series of $(Sr_{1.85}Ln_{0.15})FeMoO_6$ compounds (Ln=Sr, La, Ce, Pr, Nd, Eu and Sm), we realized that the magnetic properties of Eu-doped SFMO exhibited some anomalies [15]. Firstly, M_S of $(Sr_{1.85}Eu_{0.15})FeMoO_6$ at 5 K is smaller than that at 100 K, which is in contrast to the other rare-earth-doped SFMO. Secondly, as mentioned above, electron doping increased T_C of SFMO doped by

* Corresponding author. Fax: +86 1082649531.
E-mail address: ghrao@aphy.iphy.ac.cn (G.H. Rao).

0022-4596/$ - see front matter © 2010 Elsevier Inc. All rights reserved.
doi:10.1016/j.jssc.2010.08.013

La-, Ce-, Pr-, Nd- and Sm-doped, but the T_C of $(Sr_{1.85}Eu_{0.15})FeMoO_6$ is almost unchanged. In order to investigate systematically the effects of Eu doping on magnetic properties of SFMO, in this work we prepared a series of $(Sr_{2-x}Eu_x)FeMoO_6$ compounds ($0 \le x \le 0.3$) and studied their structural, magnetic and transport properties.

2. Experiment

Polycrystalline $(Sr_{2-x}Eu_x)FeMoO_6$ (x=0, 0.05, 0.1, 0.15, 0.2, 0.25 and 0.3) samples were prepared by standard solid-state reaction. Stoichiometric powders of $SrCO_3$, Eu_2O_3, MoO_3 and Fe_2O_3 were mixed, ground and heated at 900 °C for 5 h in air. The pre-reacted mixtures were then finely ground, pressed into pellets and sintered at 1280 °C in a flow of 5% H_2/Ar gas for 12 h with several intermediate grindings. The samples were heated and cooled at a rate of 5 °C/min under the same atmosphere.

The crystal structure and phase purity of the samples were examined by X-ray powder diffraction (XRD) using a Rigaku D/max 2500 diffractometer with Cu$K\alpha$ radiation (50 kV × 250 mA) and a graphite monochromator. The XRD data were collected in the 2θ range of 15–140° by a step-scan mode with a step width of 2θ=0.02° and a sampling time of 1 s. The XRD data were analyzed by means of the Rietveld refinement using the program FULLPROF [16,17].

The field dependence of magnetization of the compounds in the temperature range of $5\ K \le T \le 300\ K$ was measured on a quantum design superconducting quantum interference device (SQUID) magnetometer in magnetic field up to 5 or 7 T. The sample was mounted in the SQUID magnetometer using a clear plastic drinking straw. The temperature dependence of the magnetization was recorded on a vibrating-sample magnetometer (quantum design) in an applied field of 0.05 T from 300 to 500 K. The transport properties were measured by the standard four-probe method.

3. Results and discussion

Fig. 1 presents the XRD patterns of $(Sr_{2-x}Eu_x)FeMoO_6$ ($0 \le x \le 0.3$). All the compounds are of single phase without detectable impurity phases. Owing to the ordering arrangement of Fe and Mo on B and B' sites in perovskite structure, the superstructure reflection (101) for the tetragonal structure or (111) for the cubic structure (see below) is observed. However, the intensity of the superstructure reflection decreases with the doping level, indicating that Eu doping destroys the Fe/Mo ordering. The level of the anti-site defect (AS) was determined from the Rietveld refinement of the crystal structure.

The structure refinement was first performed with the space group $I4/m$, and this model gave a reasonable fit for the parent compound and $(Sr_{1.95}Eu_{0.05})FeMoO_6$. However, for the compounds with $x \ge 0.1$, the splitting of some reflections at high diffraction angles disappeared. For example, three reflections (116), (332) and (420) in the $I4/m$ lattice emerged into one reflection (inset of Fig. 2(a) and (b)). This makes it necessary to consider a higher crystal symmetry than the tetragonal one. The structure was successfully refined by $Fm\bar{3}m$ space group. This structural transition can be attributed to the cationic steric effects, which is frequently observed in perovskite manganites [18] and double perovskites [19]. The refinement results are listed in Table 1. The unit-cell volume decreases slightly with the Eu content for both the $I4/m$ and $Fm\bar{3}m$ lattices. On the one hand, as evidenced by neutron powder diffraction [11], nuclear magnetic

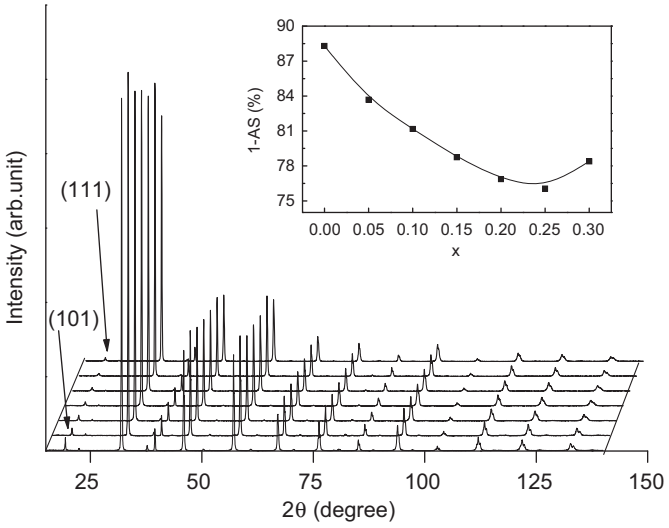

Fig. 1. XRD patterns of $(Sr_{2-x}Eu_x)FeMoO_6$. From bottom to top: x=0, 0.05, 0.1, 0.15, 0.2, 0.25 and 0.3. Arrow indicates the superstructure reflection. Inset is the degree of ordering as a function of doping level.

resonance [20] and Mössbauer [21] experiments, the doped electrons selectively entered the Mo sites and reduced part of the Mo ions from Mo^{5+} (0.61 Å) to Mo^{4+}(0.65 Å), but the ionic radius of Eu^{3+} is much smaller than that of Sr^{2+} (Eu^{3+}:1.28 Å, Sr^{2+}: 1.44 Å), thus the unit-cell volume of $(Sr_{2-x}Eu_x)FeMoO_6$ should decrease with x. On the other hand, as reported in Ref. [8], the doped electron provides delocalized carriers selectively for the spin-down t_{2g} metallic spin channel, which will increase the density of state at the Fermi level. These carriers can modify the bond lengths through screening the ionic potentials, so the unit-cell volume would be increased by electron doping. In$(Sr_{2-x}Eu_x)$-$FeMoO_6$ compound, the steric effect seems to prevail slightly over the electron doping effect, leading to the slight reduction of the unit-cell volume with the Eu content. As an example, Fig. 2(a) and (b) presents the calculated and experimental XRD profiles for $(Sr_{1.95}Eu_{0.05})FeMoO_6$ (SG: $I4/m$) and $(Sr_{1.75}Eu_{0.25})FeMoO_6$ (SG:$Fm\bar{3}m$), respectively. Consistent with the visual decrease of the intensity of the superstructure reflection, the degree of Fe/Mo ordering, 1-AS, decreases pronouncedly with the doping level (inset of Fig. 1). Similar phenomenon had been observed for other electron doped double perovskites, such as $(Sr_{2-x}La_x)FeMoO_6$ and $(Sr_{2-x}Nd_x)FeMoO_6$ [10–14]. This phenomenon is related to the differences in charge and size of the ions [22]. As mentioned above, electron doping reduced the valence of the Mo ions, while the valence of the Fe ions was almost unchanged, therefore, the charge and size difference between Fe and Mo ions were reduced and the degree of ordering decreased accordingly.

Fig. 3 shows the temperature dependence of magnetization of $(Sr_{2-x}Eu_x)FeMoO_6$ compounds in a field of 0.05 T. For the sake of clarity, all the curves are normalized at 300 K and shifted from each other. The ferromagntic–paramagnetic (FM–PM) transition is broadened with the doping level due to the increase of AS defects and possible inhomogeneity in the compounds. The transition temperature (T_C) is determined as the inflection point of the M–T curve and is listed in Table 1. In contrast to the anticipation that the electron doping should reinforce the magnetic interaction and elevate T_C [9] as evidenced in several electron-doped compounds [10–14], Eu doping seems not to increase T_C of the compounds considerably or systematically. Monte Carlo simulation study showed that both the saturation magnetization and T_C of Sr_2FeMoO_6 decreased with the increase of the AS concentration [23]. It is plausible that the reduction of T_C due to the AS defects

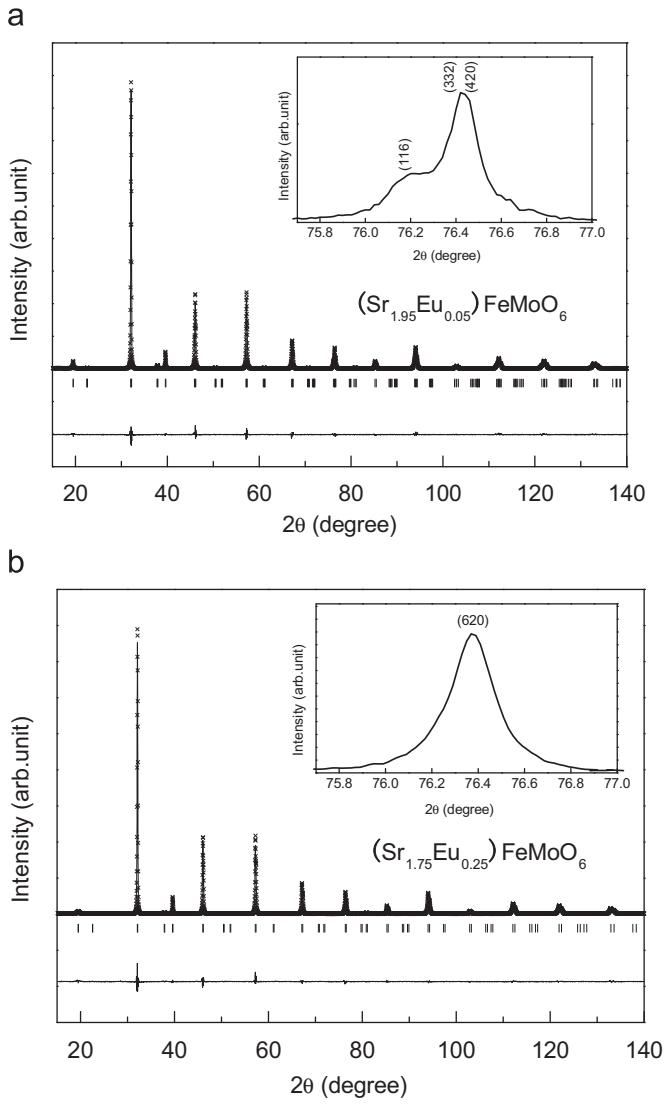

Fig. 2. Observed (crosses) and calculated (solid curve) XRD patterns: (a) $(Sr_{1.95}Eu_{0.05})FeMoO_6$, $I4/m$ lattice. (b) $(Sr_{1.75}Eu_{0.25})FeMoO_6$, $Fm\bar{3}m$ lattice. The vertical bars at the bottom indicate the Bragg reflection positions, and the lowest curve is the difference between the observed and the calculated XRD patterns. Insets are the magnified pattern around $2\theta = 76^\circ$.

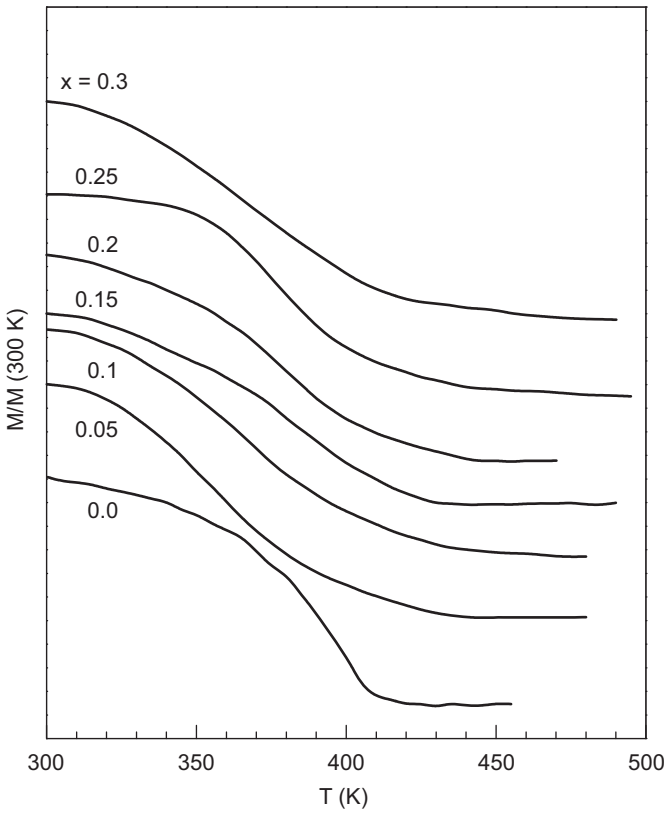

Fig. 3. Temperature dependence of the magnetization of $(Sr_{2-x}Eu_x)FeMoO_6$ in 0.05 T.

counteracts the electron doping effect in the investigated doping level.

Field dependence of magnetization of $(Sr_{2-x}Eu_x)FeMoO_6$ $(0 \le x \le 0.3)$ compounds measured at 5 K under the applied fields up to 5 T is shown in Fig. 4. The magnetization increases rapidly with the applied field and then approaches a saturation value M_S (derived by extrapolating $1/H$ to zero on the $M-1/H$ curve), indicating that all the compounds are ferromagnetic. The magnetization of the doped compound increases more slowly at low fields and the M_S is lower than the parent compound, suggesting that the ferromagnetic state of Sr_2FeMoO_6 is strongly disturbed by Eu doping.

The derived M_S of the compounds at 5 K is listed in Table 1. The M_S of $(Sr_{2-x}Eu_x)FeMoO_6$ decreases markedly with the doping level. As reported in Ref. [15], the moments of rare-earth ions could become long-range ordered at low temperature (for example, 5 K) and contribute to the M_S of $(Sr_{2-x}Eu_x)FeMoO_6$. In order to elucidate the relationship between M_S and cation ordering on the B sites, the effect of the rare-earth ions moment on M_S should be eliminated. We measured the magnetization curves at 100 K and listed the M_S value in Table 1. The linear relation between M_S of $(Sr_{2-x}Eu_x)FeMoO_6$ at 100 K and AS (inset of Fig. 5) coincides with the FIM prediction ($M_S = 4–8 \times$ AS μ_B/f.u. for Sr_2FeMoO_6), indicating that the long-range order of Eu^{3+} moments has collapsed at 100 K and the M_S value results essentially from Fe^{3+} and Mo^{5+} ions. Evolutions of M_S at 5 and 100 K with composition are shown in Fig. 5. For the compounds with $x \le 0.15$, the M_S values at 5 and 100 K are almost the same. However, for the compounds with $x > 0.15$, the M_S at 100 K is obviously larger than that at 5 K. This phenomenon may be explained in the following scenario: assuming that the moment of Eu^{3+} ion is antiparallel to that of Fe^{3+} ion, the M_S of $(Sr_{2-x}Eu_x)FeMoO_6$ will increase once the long-range order of Eu^{3+} moments collapses. The effect of rare-earth moment on the M_S will be manifested beyond the percolation threshold, which seems to be close to $x = 0.15$ for the $(Sr_{2-x}Eu_x)FeMoO_6$ compounds.

In order to confirm the arrangement of the moment of Eu^{3+} ion in $(Sr_{2-x}Eu_x)FeMoO_6$, we measured the magnetization curves of $(Sr_{1.8}Eu_{0.2})FeMoO_6$ and $(Sr_{1.8}Nd_{0.2})FeMoO_6$, which were synthesized under the same conditions, at different temperatures ($T = 5$, 10, 20, 30, 40, 50, 60, 70, 80, 90, 100, 150, 200, 250 and 300 K) and under the applied fields up to 7 T. As an example, the magnetization curves at 5, 60, 100, 200 and 300 K are shown in Fig. 6(a) and (b). The derived M_S of $(Sr_{1.8}Eu_{0.2})FeMoO_6$ at different temperatures are shown in Fig. 7 as filled circles. As temperature increases, the M_S increases gradually, reaches a maximum value of 2.25 μ_B/f.u. around 60 K and then decreases monotonically, suggesting that the long-range ordering of the Eu^{3+} moments collapses around $T = 60$ K. Similar feature is observed on the thermomagnetic curve (inset of Fig. 7). In contrast, the temperature dependence of M_S of $(Sr_{1.8}Nd_{0.2})FeMoO_6$ exhibits an upturn around 30 K (open circles in Fig.7). However, the M_S of two

Table 1
Lattice and atomic parameters, degree of Fe/Mo ordering ($\eta = 1 - AS$), temperature factor (B), reliability indexes (R_{wp}, R_e), Curie temperature (T_C) and saturation magnetization (M_S) of $(Sr_{2-x}Eu_x)FeMoO_6$. For $x \le 0.05$, the compounds belong to $I4/m$ lattice, Sr/Eu ion is located at 4d ($\frac{1}{2}\ 0\ \frac{1}{4}$), Fe at 2$a$ (000) and Mo at 2b ($00\frac{1}{2}$). For $x \ge 0.1$, the compounds belong to $Fm\bar{3}m$ lattice, Sr/Eu ion is located at 8c ($\frac{1}{4}\ \frac{1}{4}\ \frac{1}{4}$), Fe at 4$a$ (000) and Mo at 4b ($\frac{1}{2}\ \frac{1}{2}\ \frac{1}{2}$). Only the atomic parameters of oxygen are listed in the table.

	$x=0$	$x=0.05$	$x=0.1$	$x=0.15$	$x=0.2$	$x=0.25$	$x=0.3$
Space group	$I4/m$	$I4/m$	$Fm\bar{3}\ m$	$Fm\bar{3}\ m$	$Fm\bar{3}\ m$	$Fm\bar{3}\ m$	$Fm\bar{3}\ m$
a (Å)	5.5745(1)	5.5735(1)	7.8853(1)	7.8834(1)	7.8826(1)	7.8819(1)	7.8822(1)
c (Å)	7.8986(1)	7.8976(1)	7.8853(1)	7.8834(1)	7.8826(1)	7.8819(1)	7.8822(1)
V (Å^3)	245.45(1)	245.33(1)	490.31(1)	489.95(1)	489.78(1)	489.67(1)	489.73(1)
η (%)	88.31(1)	83.61(3)	81.22(2)	78.80(3)	76.91(1)	76.30(1)	78.42(1)
AS (%)	11.69(1)	16.39(3)	18.78(2)	21.20(3)	23.09(1)	23.70(1)	21.58(1)
O_1 8h ($xy0$)							
x	0.2752(6)	0.2724(21)	–	–	–	–	–
y	0.2281(4)	0.2293(13)	–	–	–	–	–
O_2 4e (00z)							
z	0.2582(8)	0.2607(25)	–	–	–	–	–
O_1 24e ($x00$)							
x	–	–	0.2522(4)	0.2517(4)	0.2512(1)	0.2512(1)	0.2507(1)
$B_{Sr/Eu}$ (Å^{-2})	0.49(1)	0.57(2)	0.58(2)	0.57(2)	0.58(1)	0.54(1)	0.55(1)
B_{Fe} (Å^{-2})	0.13(1)	0.13(4)	0.22(4)	0.28(1)	0.31(1)	0.28(1)	0.24(1)
B_{Mo} (Å^{-2})	0.04(1)	0.02(1)	0.001(1)	0.004(3)	0.003(2)	0.003(2)	0.0007(5)
R_{wp} (%)	12.6	13.1	13.4	13.4	13.3	13.4	12.4
R_e (%)	7.07	7.00	7.22	7.29	7.51	7.72	7.64
T_C (K)	412	397	408	416	414	410	416
M_S 5 K (μ_B/f.u.)	3.26	2.81	2.49	2.21	1.92	1.64	1.85
M_S 100 K (μ_B/f.u.)	3.25	2.75	2.45	2.24	2.12	1.95	2.13

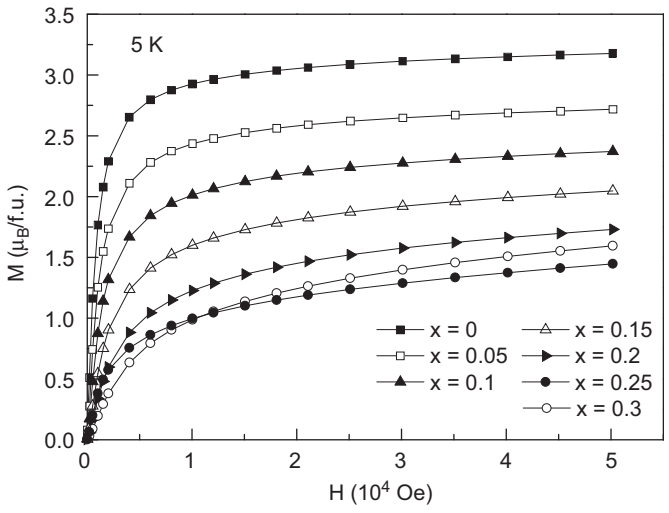

Fig. 4. Magnetization curves of $(Sr_{2-x}Eu_x)FeMoO_6$ at 5 K.

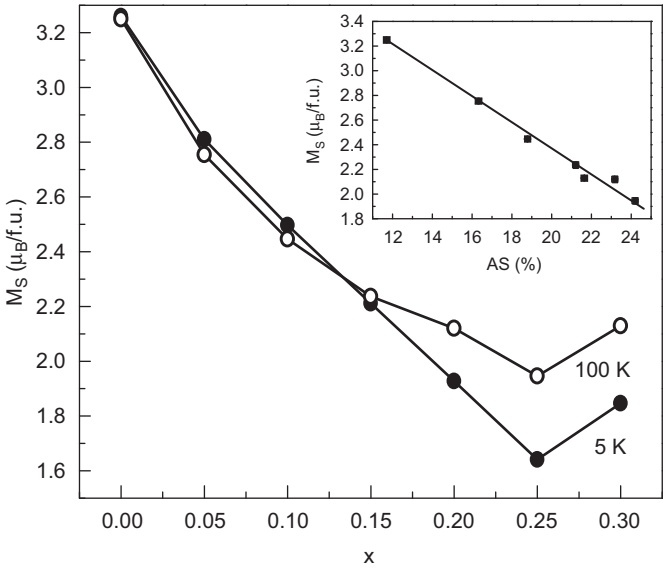

Fig. 5. Composition dependence of saturation magnetization at 5 K (filled circle) and 100 K (open circle). Inset shows the relation between the saturation magnetization at 100 K and the anti-site defect concentration.

compounds is close to each other above 100 K, which is indication of an almost absence of the influence arising from the rare earth doping and further corroborates that the contribution of the long-rang ordering of the rare earth moments takes effect essentially at low temperature. The comparison shown in Fig. 7 implies that the magnetic coupling between Nd and Fe is different from that between Eu and Fe, which warrants further investigations.

Temperature dependence of the normalized resistivity of the compounds from 5 to 300 K is shown in Fig. 8. Depending on the synthesis conditions, SFMO can exhibit insulating, semiconducting or metallic behaviors [24]. In our case, both parent compound and the doped compounds exhibit a metal–semiconductor (M–S) transition, and the transition temperature (T_{M-S}) is indicated by upward arrows in Fig.8. Similar M–S transition had been observed in $Sr_2(Fe_{1-x}Cr_x)MoO_6$ [25], $(Sr_{2-3x}La_{2x}Ba_x)FeMoO_6$ [26] and $Sr_2(Fe_{1-x}V_x)MoO_6$ [27] compounds. For the investigated $(Sr_{2-x}Eu_x)FeMoO_6$ compounds, both the resistivity and T_{M-S} increase with the Eu content, which seems to associate with the increased anti-site defects concentration and inhomogeneity that enhance scattering of the carriers at low temperature.

4. Conclusion

The electron doped double perovskite compounds $(Sr_{2-x}Eu_x)FeMoO_6$ ($0 \le x \le 0.3$) have been prepared by solid-state reaction. All the compounds are of single phase and the unit-cell volume decreases slightly with the doping level. XRD experiments and Rietveld refinements of crystal structure reveal that the crystal structure of $(Sr_{2-x}Eu_x)FeMoO_6$ transforms from $I4/m$ lattice to

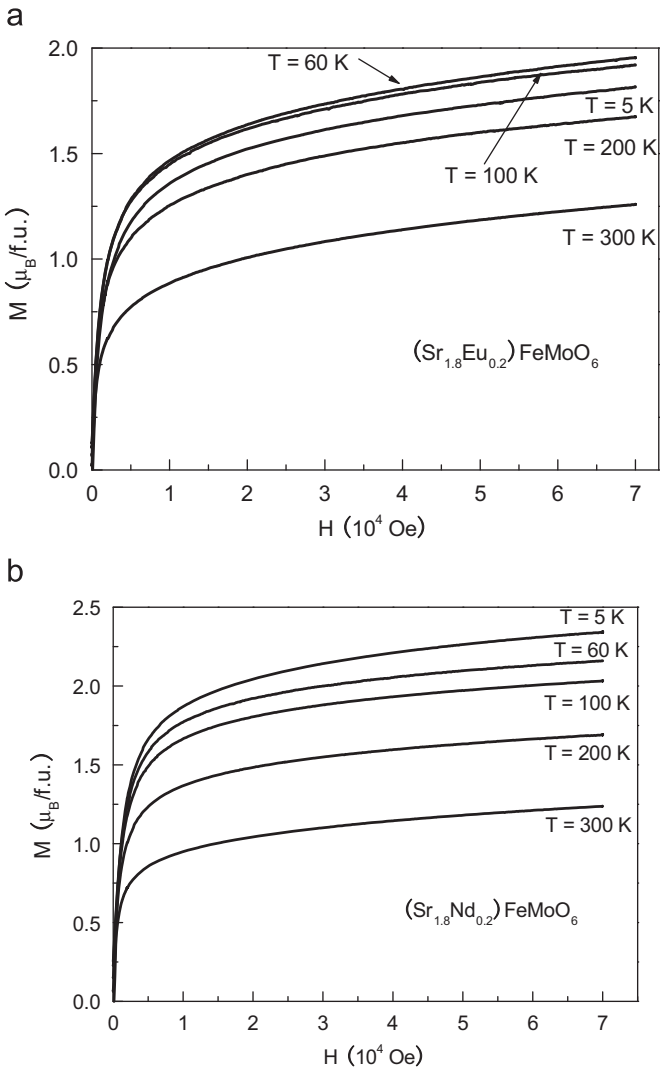

Fig. 6. Magnetization curves of (a) $(Sr_{1.8}Eu_{0.2})FeMoO_6$ and (b) $(Sr_{1.8}Nd_{0.2})FeMoO_6$ at 5, 60, 100, 200 and 300 K.

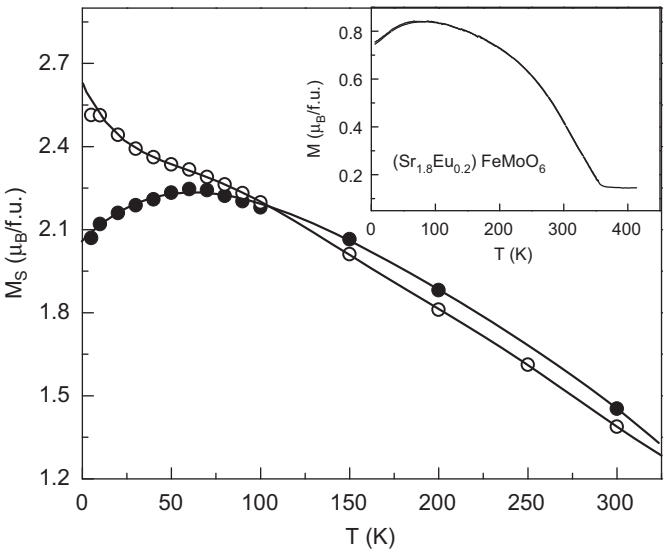

Fig. 7. Temperature dependence of saturation magnetization of $(Sr_{1.8}Eu_{0.2})FeMoO_6$ (filled circle) and $(Sr_{1.8}Nd_{0.2})FeMoO_6$ (open circle). Inset shows the temperature dependence of the magnetization of $(Sr_{1.8}Eu_{0.2})FeMoO_6$ under an applied field of 0.2 T.

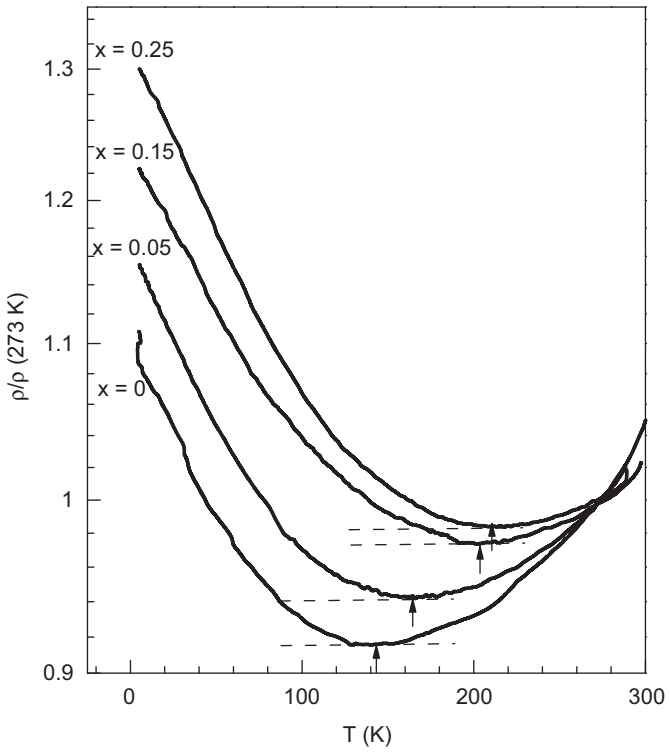

Fig. 8. Temperature dependence of the normalized resistivity of the compounds with $x=0$, 0.05, 0.15 and 0.25. The dashed horizontal lines manifest the changeover of the resistivity behavior around the metal–semiconductor transition temperature indicated by the arrow.

$Fm\bar{3}m$ lattice around $x=0.1$. As the doping increases, the cation ordering on the B sites is decreased markedly and the saturation magnetization (M_S) of the compounds is reduced accordingly, whereas the Curie temperature is almost unchanged. A linear relation between the anti-site defects concentration (AS) and M_S at 100 K is observed. Comparison of the M_S between 5 and 100 K indicates that the moment of Eu^{3+} ion is long-rang ordered at low temperature and antiparallel to that of Fe^{3+} ion. Both parent compound and the doped compounds exhibit a metal–semiconductor (M–S) transition, and the resistivity and T_{M-S} increase with the Eu content.

Acknowledgments

This work was supported by the National Basic Research Project of MOST (Grant no. 2007CB925003) and by the National Natural Science Foundation of China (Grant no. 50872148).

References

[1] K.-I. Kobayashi, T. Kimura, H. Sawada, K. Terakura, Y. Tokura, Nature 395 (1998) 677.
[2] D.D. Sarma, P. Mahadevan, T. Saha-Dasgupta, S. Ray, A. Kumar, Phys. Rev. Lett. 85 (2000) 2549.
[3] D.D. Sarma, E.V. Sampathkumaran, S. Ray, R. Nagarajan, S. Majumdar A. Kumar, G. Nalini, T.N.G. Row, Solid State Commun. 114 (2000) 465.
[4] K.-I. Kobayashi, T. Kimura, Y. Tomioka, H. Sawada, K. Terakura, Y. Tokura, Phys. Rev. B 59 (1999) 11159.
[5] C. Ritter, M.R. Ibarra, L. Morellon, J. Blasco, J. García, J.M. De Teresa, J. Phys.: Condens. Matter 12 (2000) 8295.
[6] R.P. Borges, R.M. Thomas, C. Cullinan, J.M.D. Coey, R. Suryanarayanan, L. Ben-Dor, L. Pinsard-Gaudart, A. Revcolevschi, J. Phys.: Condens. Matter 11 (1999) L445.
[7] L.I. Balcells, J. Navarro, M. Bibes, A. Roig, B. Martínez, J. Fontcuberta, Appl. Phys. Lett. 78 (2001) 781.

[8] J. Navarro, C. Frontera, L.I. Balcells, B. Martínez, J. Fontcuberta, Phys. Rev. B 64 (2001) 092411.
[9] M. Tovar, M.T. Causa, A. Butera, J. Navarro, B. Martinez, J. Fontcuberta, M.C.G. Passeggi, Phys. Rev. B 66 (2002) 024409.
[10] D. Rubi, C. Frontera, G. Herranz, J.L.G. Muñoz, J. Fontcuberta, C. Ritter, J. Appl. Phys. 95 (2004) 7082.
[11] C. Frontera, D. Rubi, J. Navarro, J.L. García-Muñoz, J. Fontcuberta, Phys. Rev. B 68 (2003) 012412.
[12] A.K. Azad, S.G. Eriksson, K. Abdullah, A. Riksson, M. Tseggai, J. Solid State Chem. 179 (2006) 1303.
[13] E.K. Hemery, G.V.M. Williams, H.J. Trodahl, Phys. Rev. B 74 (2006) 054423.
[14] D. Rubi, C. Frontera, J. Nogués, J. Fontcuberta, J. Phys.: Condens. Matter 16 (2004) 3173.
[15] Q. Zhang, G.H. Rao, Y.G. Xiao, H.Z. Dong, G.Y. Liu, Y. Zhang, J.K. Liang, Physica B 381 (2006) 233.
[16] R.A. Young, D.B. Wiles, J. Phys. Cryst. 15 (1982) 430.
[17] J. Rodroguez-Carvajal, Physica B 192 (1993) 55.
[18] P.G. Radaelli, G. Iannone, M. Marezio, H.Y. Hwang, S.W. Cheong, J.D. Jorgensen, D.N. Argyriou, Phys. Rev. B 56 (1997) 8265.
[19] Q.D. Zhou, B.J. Kennedy, M.M. Elcomb, J. Solid State Chem. 180 (2007) 541.
[20] M. Wojcik, E. Jedryka, S. Nadolski, J. Navarro, D. Rubi, J. Fontcuberta, Phys. Rev. B 69 (2004) 100407R.
[21] J. Lindén, T. Shimada, T. Motohashi, H. Yamauchi, M. Karppinen, Solid State Commun. 129 (2004) 129.
[22] M.T. Anderson, K.B. Greenwood, G.A. Taylor, K.R. Poppelmeier, Prog. Solid State Chem. 22 (1993) 197.
[23] A.S. Ogale, S.B. Ogale, R. Ramesh, T. Venkatesan, Appl. Phys. Lett. 75 (1999) 537.
[24] M. Itoh, I. Ohta, Y. Inaguma, Mater. Sci. Eng. B 41 (1996) 55.
[25] X.M. Feng, G.H. Rao, G.Y. Liu, H.F. Yang, W.F. Liu, Z.W. Ouyang, J.K. Liang, Physica B 344 (2004) 21.
[26] Q. Zhang, G.H. Rao, H.Z. Dong, Y.G. Xiao, X.M. Feng, G.Y. Liu, Y. Zhang J.K. Liang, Physica B 370 (2005) 228.
[27] Q. Zhang, G.H. Rao, X.M. Feng, G.Y. Liu, Y.G. Xiao, Y. Zhang, J.K. Liang, Solid State Commun. 133 (2005) 223.